Toward Olefin Multiblock Copolymers with Tailored Properties: A Molecular Perspective

Yousef Mohammadi, Mohammad Reza Saeb, Alexander Penlidis, Esmaiel Jabbari, Florian J. Stadler, Philippe Zinck, Eduardo Vivaldo-lima, Krzysztof Matyjaszewski

Towards Olefin Multi-block Copolymers with Tailored Properties: A Molecular Perspective

Yousef Mohammadi[1]*, Mohammad Reza Saeb[2], Alexander Penlidis[3]*, Esmaiel Jabbari[4], Florian J. Stadler[5]*, Philippe Zinck[6], Eduardo Vivaldo-Lima[7], Krzysztof Matyjaszewski[8]*

[1] Petrochemical Research and Technology Company (NPC-rt), National Petrochemical Company (NPC), P.O. Box 14358-84711, Tehran, Iran

[2] Department of Resin and Additives, Institute for Color Science and Technology, P.O. Box 16765-654, Tehran, Iran

[3] Department of Chemical Engineering, Institute for Polymer Research (IPR), University of Waterloo, Waterloo, Ontario N2L 3G1, Canada

[4] Biomimetic Materials and Tissue Engineering Laboratory, Department of Chemical Engineering, University of South Carolina Columbia, SC 29208, USA

[5] College of Materials Science and Engineering, Shenzhen Key Laboratory of Polymer Science and Technology, Guangdong Research Center for Interfacial Engineering of Functional Materials, Nanshan District Key Lab for Biopolymers and Safety Evaluation, Shenzhen University, Shenzhen 518060, China

[6] Univ. Lille, CNRS, Centrale Lille, Univ. Artois, UMR 8181 - UCCS - Unité de Catalyse et Chimie du Solide, F-59650 Villeneuve d'Ascq, France.

[7] Facultad de Química, Departamento de Ingeniería Química, Universidad Nacional Autónoma de México, CU, 04510, México City, México

[8] Department of Chemistry, Carnegie Mellon University, Pittsburgh, PA 15213, USA

To whom correspondence should be addressed:

Dr. Yousef Mohammadi: mohammadi@npc-rt.ir

Prof. Alexander Penlidis: penlidis@uwaterloo.ca

Prof. Florian J. Stadler: fjstadler@szu.edu.cn

Prof. Krzysztof Matyjaszewski: matyjaszewski@cmu.edu

ABSTRACT

Recent progress in macromolecular reaction engineering has enabled the synthesis of sequence-controlled polymers. The advent of Olefin Block Copolymers (OBCs) via chain shuttling polymerization of ethylene with α-olefins has opened new horizons for the synthesis of polyolefins having a dual character of thermoplastics and elastomers. Nevertheless, the use of two catalysts with different comonomer selectivities and a chain shuttling agent, dragging and dropping live chains between active catalyst centers, made precise tailoring of OBCs microstructure containing hard and soft units a feasible challenge. This work discusses the possibility of predicting properties of OBCs from its simulated molecular patterns. The microstructural characteristics of OBCs are discussed in terms of topology-related and property-related features. An intelligent tool, which combines the benefits of Kinetic Monte Carlo simulation and Artificial Neural Network modeling, was used to explore the connection between polymerization recipe (catalyst composition, ethylene to 1-octene monomer ratio, and chain shuttling agent level) and topology-related as well as property-related microstructural features. The properties of target OBCs are reflected in the hard block percent, the number of 1-octene units in the copolymer chains, and the longest ethylene sequence length of the hard and soft segments.

1. INTRODUCTION

Understanding the complex interrelationships between polymerization formulation (recipe), microstructure, and ultimately the polymer properties is the key to tailor-making complex macromolecules [1-3]. However, available theoretical and experimental techniques are not capable of appropriately addressing the complexities of producing tailor-made macromolecules. Experimental analyses alone cannot capture multifaceted aspects of complex polymerization kinetics, owing to interrelated factors and the inability of current analytical Instruments to quantify the detailed microstructure of synthesized macromolecules. This knowledge could qualitatively give rise to the correlation between operating variables and ultimate properties of polymers, but the microstructure of polymers could only be very roughly identified. On the other hand, the use of classical deterministic mathematical modeling approaches could similarly provide a general understanding of the topology of macromolecules but without detailed information about every individual polymer chain in the polymerization media. Thus, available experimental and theoretical approaches could not be expected to be capable of precisely tailoring complex macromolecules. The problem would become more multidimensional in case of copolymers and/or multi-block macromolecules, where properties of polymers are determined by the concentration and the position of monomers of each type along the blocks and/or copolymer chains [4,5].
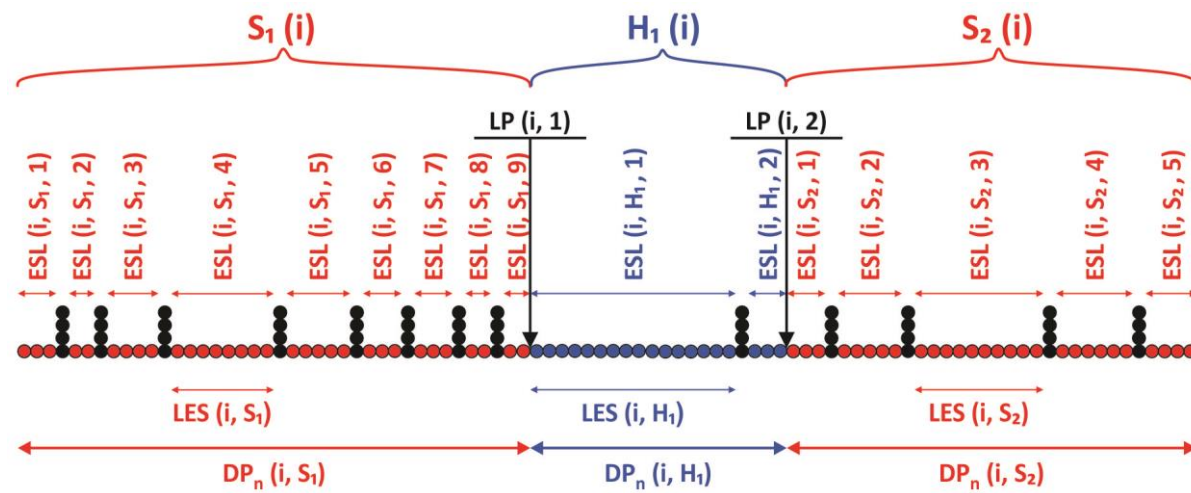
Olefin Block Copolymers (OBCs) are special-purpose polyolefins resulting from chain shuttling copolymerization of ethylene with α-olefins [6]. They exhibit properties of thermoplastics and elastomers due to hard and soft segments incorporated in their microstructure [7-13]. As a result, the microstructure of OBCs can be expressed by a large set of molecular indices, whose direct correlation with operating conditions (amount and type of catalysts and monomers, and concentration of chain shuttling agent) and ultimate properties is poorly understood. Compared to classical polyolefin synthesis, complexities of chain shuttling polymerization necessitate an advanced understanding of polymerization kinetics and evolution of microstructural indicators in the course of the polymerization [14].

The microstructural characteristics of OBCs can be classified into two categories: (*i*) topology-related molecular variables, including the number of linkage points per chain (LP), the average degree of polymerization of soft segments ($\overline{DP_n}^{SOFT}$), the average degree of

polymerization of hard segments ($\overline{DP}_n^{HARD}$), ethylene sequence length of soft segments ($\overline{ESL}^{SOFT}$), and ethylene sequence length of hard segments ($\overline{ESL}^{HARD}$); and (*ii*) property-related molecular variables, including the comonomer content of the soft segments ($\overline{C8\%}^{SOFT}$), comonomer content of the hard segments ($\overline{C8\%}^{HARD}$), the average longest ethylene sequence length of the soft blocks ($\overline{LES}^{SOFT}$), the average longest ethylene sequence length of the hard blocks ($\overline{LES}^{HARD}$), and hard block percentage ($HB\%$) [15]. The topology-related characteristics were comprehensively discussed in a previous publication by patterning macromolecular landscape of OBCs [16]. Nevertheless, there is sufficient evidence that physical, thermal, rheological, and mechanical properties of OBCs are mostly controlled by the characteristics of the second group.

The schematic of a typical OBC chain is illustrated in Figure 1, in which all the molecular characteristics of a tri-block copolymer number i are shown. The presented tri-block OBC chain contains two soft blocks, denoted as S1 and S2, and one hard block, denoted as H1, taking an average number of linkage points per chain (LP) of 2. It is well-documented that the Flory-Huggins interaction parameter (χ) is correlated with the difference between 1-octene content of the soft and hard blocks ($\Delta\overline{C8\%}$) [17,18]. In the case of a typical OBC chain shown in Figure 1, the $\overline{C8\%}^{HARD}$ of H1 block takes on the value of 5.00%, considering that one 1-octene unit exists in the H1 block having 19 ethylene units. In a similar fashion, $\overline{C8\%}^{SOFT}$ of S1 and S2 blocks take on the values of 20.00% and 12.50% for soft blocks having 32 and 28 ethylene units (along with 8 and 4 1-octene units), respectively. Moreover, the $\overline{C8\%}$ values of soft blocks, hard block, and the tri-block OBC chain are 16.67%, 5.00%, and 14.13%, respectively. As a result, the $\Delta\overline{C8\%}$ calculated for tri-block OBC is 11.67%, which can be considered as a low content that narrows the processing window. Studies have revealed that crystallization of OBCs in hard-block-rich or soft-block-rich phases is strongly related to $\Delta\overline{C8\%}$ [19]. A large $\Delta\overline{C8\%}$ normally facilitates mesophase separation in the melt and, hence, it could be a measure of crystallization mode. In contrast, the mesophase separation phenomenon was hardly observed for OBCs having small $\Delta\overline{C8\%}$ values [20]. However, the level of phase segregation strongly depends on the $HB\%$ of OBCs, e.g. a value of 17.56 for a typical tri-block OBC of Figure 1. A small $HB\%$ decreases the crystallization temperature and

helps mesophase separation to take place. However, depending on their values, $\overline{DP_n}^{SOFT}$ and $\overline{DP_n}^{HARD}$ (40 and 32, respectively, for S1 and S2 blocks, 20 for H1 block, and 92 for the tri-block OBC) may overwhelm the $HB\%$ effect. There is evidence that rheological behavior is sensitive to mesophase separation [21-25]. In addition, $\overline{LES}^{SOFT}$ and $\overline{LES}^{HARD}$ can also contribute to the crystallization behavior of OBCs [26-32]. Accordingly, the above-discussed characteristics are correctly defined as property-related molecular variables of OBCs.

Figure labels (top to bottom):

S₁(i)   H₁(i)   S₂(i)

LP(i, 1)   LP(i, 2)

ESL(i, S₁, 1), ESL(i, S₁, 2), ESL(i, S₁, 3), ESL(i, S₁, 4), ESL(i, S₁, 5), ESL(i, S₁, 6), ESL(i, S₁, 7), ESL(i, S₁, 8), ESL(i, S₁, 9), ESL(i, H₁, 1), ESL(i, H₁, 2), ESL(i, S₂, 1), ESL(i, S₂, 2), ESL(i, S₂, 3), ESL(i, S₂, 4), ESL(i, S₂, 5)

LES(i, S₁)   LES(i, H₁)   LES(i, S₂)

DPₙ(i, S₁)   DPₙ(i, H₁)   DPₙ(i, S₂)

	First Soft Block	First Hard Block	Second Soft Block	Total Soft Blocks	Total Hard Blocks	OBC Chain
Symbol	$S_1(i)$	$H_1(i)$	$S_2(i)$	$S(i)$	$H(i)$	$OBC(i)$
Number of ethylene units	32	19	28	60	19	79
Number of 1-octene units	8	1	4	12	1	13
$\overline{LP}$	-	-	-	-	-	2
$\overline{DP_n}$	40	20	32	-	-	92
$\overline{ESL}$ s (Left-to-Right)	3-2-4-8-5-3-3-2-2	16-3	3-5-10-6-4	-	-	-
$\overline{C}8\%$	20.00	5.00	12.50	16.67	5.00	14.13
$\Delta\overline{C}8\%$	-	-	-	-	-	11.67
$\overline{LES}$	8	16	10	10	16	16
$HB\%$	-	-	-	-	-	17.56

Figure 1. Detailed view of a typical tri-block OBC chain with two soft blocks, S1 and S2, and one hard block, H1, which demonstrates microstructural features of LP, $\overline{DP_n}$, $\overline{ESL}$, $\overline{C}8\%$, $\overline{LES}$, and $HB\%$ for blocks and chains.

At this point, one should note that property-related molecular indicators cannot be easily measured through experimental analyses. In other words, a simple 1:1 relation cannot be found between the polymerization recipe, microstructure, and properties of OBCs. Kinetic Monte Carlo (KMC) simulations of chain shuttling polymerizations of ethylene and 1-octene enabled virtual synthesis of OBCs [33-35]. For tailoring OBCs, in view of the complexities with chain shuttling polymerization and the diversity of molecular indices to be captured and optimized, one may need to virtually copolymerize ethylene and α-olefins over a wide range of synthesis conditions, which seems a near-to-impossible task considering time requirements of the KMC simulator. Previously, we developed an Intelligent Modeling Tool (IMT) by hybridizing Artificial Neural Network (ANN) modeling with the KMC simulation approach [15]. The IMT is capable of imitating, screening, and generalizing the information obtained from batches synthesized by the KMC simulator (literally, thousands of scenarios never virtually synthesized before). In support of the KMC simulator, the IMT offers a fast solution to obtain and analyze the simulation results.

In the light of the above, prediction of rheological, mechanical, and thermal behavior of OBCs is pertinent to understanding the relationship between polymerization recipe, microstructure, and properties of such a complex copolymerization system. The IMT allows for virtual production of diverse OBCs for which wider ranges of polymerization recipes are correlated to microstructural patterns. This allows the identification of better correlation between operational conditions and microstructure of OBCs. In this work, a quantitative correlation is provided between operational conditions and property-related molecular characteristics of OBCs, to deepen our understanding of microstructure-property relationships in OBCs.

2. THEORETICAL BACKGROUND

In a series of prior publications, a robust and computationally efficient KMC simulator was developed and put into practice [33-35]. The well-tested KMC simulator is capable of virtually synthesizing OBC chains and monitoring/reporting the whole set of instantaneous and cumulative microstructural features (as discussed before) of the produced OBCs for all polymerization recipes examined. The input kinetic parameters required for the simulations are based on a well-known mathematical model developed and published by DOW Chemical

Company [14]. The KMC simulator could capture both topology- and property-related molecular characteristics of OBCs for a virtual (batch or semi-batch) chain shuttling coordination copolymerization process of ethylene and 1-octene. Though the results were reliable, the algorithm required a rather long time for arriving at the output for each virtual batch. Hence, in a previous work [16], the molecular landscape of OBCs was uncovered employing the IMT, which assisted the KMC simulator in finding topology-related molecular variables including LP, $\overline{DP_n}^{SOFT}$, $\overline{DP_n}^{HARD}$, $\overline{ESL}^{SOFT}$, and $\overline{ESL}^{HARD}$. The results enabled identifying new grades of OBCs having unexplored architectures. Nevertheless, the KMC algorithm required ca. 10 h to arrive at these molecular characteristics of each OBC synthesized in a virtual reactor. Therefore, finding the 1:1 relation between the polymerization recipes and topology-related molecular indicators from such a limited range of data for desired OBCs proved to be very difficult. The ANN, as an advanced intelligent computational tool, assisted the KMC simulator in finding such a complex interplay between the polymerization recipe and topology-related features of OBCs. For details on the methodology, the reader is referred to [16].

In this work, a new IMT was developed to find the property-related molecular variables including $\overline{C8\%}^{SOFT}$, $\overline{C8\%}^{HARD}$, $\overline{LES}^{SOFT}$, $\overline{LES}^{HARD}$, and $HB\%$. The polymerization recipes were the monomer ratio (MR, which represents the molar ratio of ethylene to 1-octene: 0.05 (lowest 1-octene content), 0.25, 0.50, 0.75, 0.95 (highest 1-octene content)), the catalyst composition (CC, which represents the molar ratio of Catalyst 1 (Hf-based) to Catalyst 2 (Zr-based): 0.05, 0.25, 0.50, 0.75, 0.95), and the chain shuttling agent levels (log(CSA level): -3, -2, -1, 0, +1, +2, +3; the CSA Level represents the quantity of the $ZnEt_2$ CSA used in this work divided by the reference quantity equal to 8.05×10^{-4} mol.L^{-1}). The assigned levels for operating conditions were in complete agreement with the previous work applied in obtaining topology-related molecular variables for the sake of a fair comparison. Therefore, in the first step, 175 OBCs were synthesized using the KMC simulator and their property-related features were captured. In the second step, applying the generated dataset, five ANNs were developed, trained, and tested to enable imitating the nonlinear behavior of $\overline{C8\%}^{SOFT}$, $\overline{C8\%}^{HARD}$, $\overline{LES}^{SOFT}$, $\overline{LES}^{HARD}$, and $HB\%$ in terms of log(CSA Level), CC, and MR operating factors. Some typical OBCs with their corresponding property-related features obtained by the KMC simulator are given in Table 1.

	Inputs/Operating conditions			Outputs/Microstructural features				
	X1	X2	X3	Y1	Y2	Y3	Y4	Y5
Scenario No.	MR	CC	Log(CSA Level)	$\overline{C8\%}^{SOFT}$	$\overline{C8\%}^{HARD}$	$\overline{LES}^{SOFT}$	$\overline{LES}^{HARD}$	$HB\%$
45	0.25	0.25	-1	47.18	3.16	10.65	122.28	55.56
46	0.25	0.25	0	47.31	3.53	8.74	79.52	54.63
47	0.25	0.25	+1	47.21	8.62	8.24	60.07	54.50
59	0.25	0.75	-1	44.55	3.20	10.87	115.62	8.92
60	0.25	0.75	0	44.52	4.41	8.05	58.26	9.73
61	0.25	0.75	+1	44.54	16.02	7.32	47.60	14.49
115	0.75	0.25	-1	4.50	0.21	110.43	961.85	35.88
116	0.75	0.25	0	4.51	0.26	68.38	232.43	37.73
117	0.75	0.25	+1	4.99	1.09	38.46	36.62	36.13
129	0.75	0.75	-1	2.68	0.31	270.58	565.71	6.50
130	0.75	0.75	0	2.68	0.47	178.12	124.49	6.21
131	0.75	0.75	+1	2.69	2.20	104.42	30.02	6.53
Reference[6]	0.53	0.60	0	11.86	1.36	35.23	88.93	16.19

The reference batch in Table 1 corresponds to the experimental batch published by DOW Chemical Company, for which property-related molecular characteristics are given for comparisons with that pioneering work. The results of the first stage, i.e. the KMC simulation outputs, were fed into five ANNs, and training and test procedures were completed until the desired error values were attained. As described in a series of previous publications [16, 36-41], the ANNs are able to precisely and accurately predict scenarios never experienced before through experiments or simulation. The power of hybrid KMC and ANN stochastic approaches was reflected in the newly developed IMT module developed in this work; in addition, calculation time decreased on average from hours to just seconds.

3. RESULTS AND DISCUSSION

3.1. Verification of the IMT predictions

There are some well-documented criteria for assessing whether the ANN predictions are trustworthy. The comparisons of ANN outcomes and KMC simulator outputs at identical operating conditions allow one to explore whether or not the developed ANNs imitated properly the chain shuttling kinetics. Figure 2 shows the training process of the five neural networks constructed based on datasets received from the KMC simulator. It should be noted that the training process is handled via the mean squared error (MSE) which is defined in Supporting Information through Equations (S1) and (S2). As can be seen in the figure, the

ANNs developed for prediction of $\overline{C8\%}^{SOFT}$, $\overline{C8\%}^{HARD}$, $\overline{LES}^{SOFT}$, $\overline{LES}^{HARD}$, and $HB\%$ are well trained and their MSEs follow an abrupt descending trend versus iteration, which is an obvious measure of the correctness of modeling.
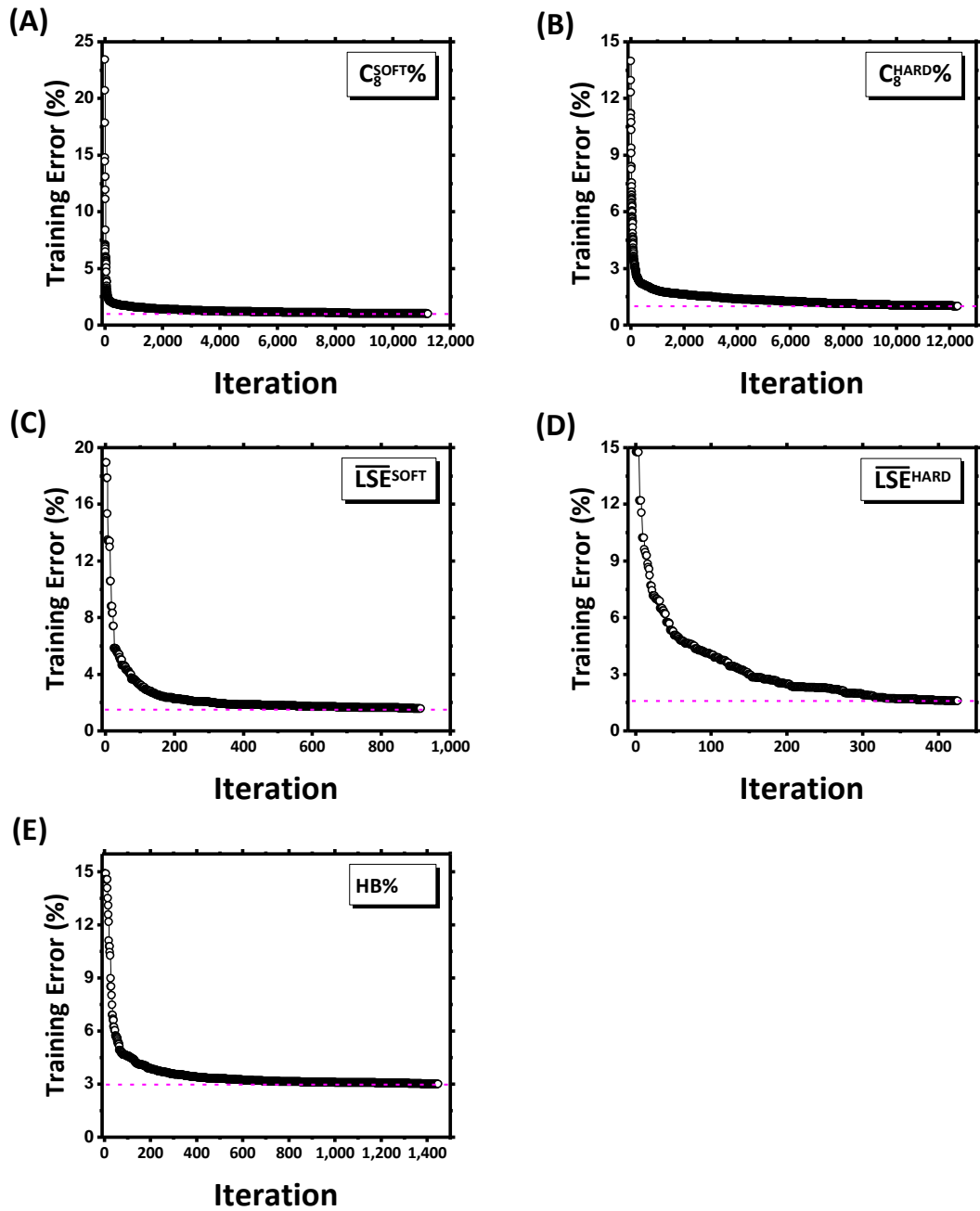

Figure 2. Iteration-dependence error in training phase of ANN modeling for (A) $\overline{C8\%}^{SOFT}$, (B) $\overline{C8\%}^{HARD}$, (C) $\overline{LES}^{SOFT}$, (D) $\overline{LES}^{HARD}$, and (E) $HB\%$.

Figure 3 compares ANN predictions for property-related variables with the corresponding values obtained by the KMC simulator at identical polymerization recipes and operating conditions. Since in the plot of the KMC results (x axis) versus the outcomes from each ANN (y axis) all data points are positioned in the vicinity of a 45° line, the developed ANNs were adequately successful in predicting property-related molecular characteristics with sufficiently small MSEs, as in Table 2. All the plots of Figure 3 are indicative of the reliability of the modeling process. All networks indicate successful training and test steps on account of training and test errors calculated for each molecular feature in Table 2.

Table 2 also lists other statistical criteria, normally used for evaluation of ANN performance, calculated using the code developed in this work. It is apparent that the maximum error in training and test procedures reported by the code is very low (Table 2). Moreover, the values of the coefficient of determination, correlation coefficient, and coefficient of efficiency for different ANNs constructed based on the data received from the KMC simulator are close to unity suggesting an adequate precision. Based on the various diagnostic criteria defined in Table 2, there is no doubt that the developed IMT can properly capture property-related features of OBCs, including interpolating for cases not being exactly covered by the KMC simulator.
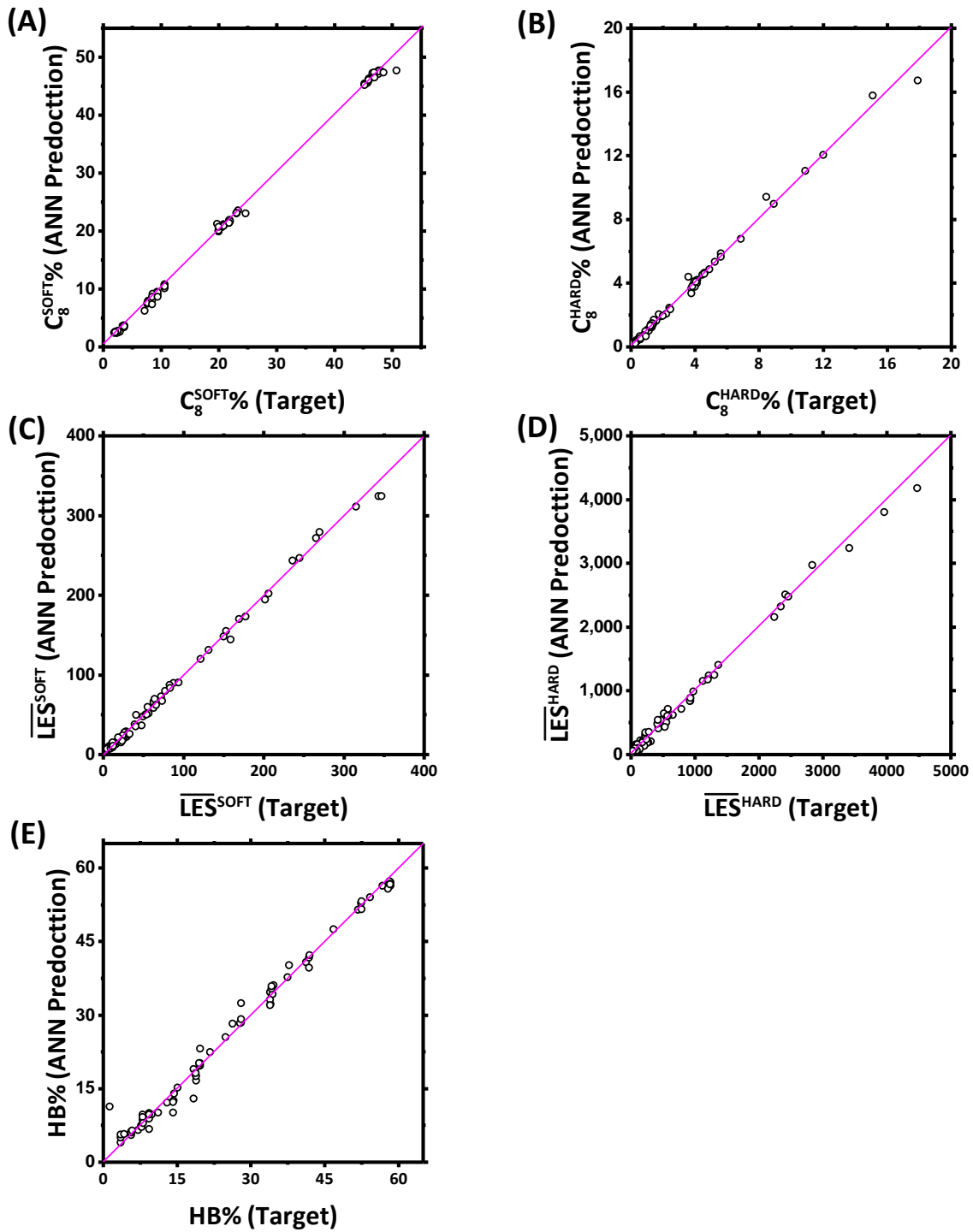
Figure 3. Analysis of the quality of the ANN predictions in comparison to the outcomes of the KMC simulator under identical conditions.

Table 2. Results of statistical analyses devoted to training and test procedures applied in ANN modeling.

	$Y1:\overline{C_8}^{SOFT}$	$Y2:\overline{C_8}^{HARD}$	$Y3:\overline{LES}^{SOFT}$	$Y4:\overline{LES}^{HARD}$	$Y5:HB\%$
Training MSE	0.00040	0.00040	0.00100	0.00099	0.00360
Test MSE	0.00078	0.00133	0.00098	0.00102	0.00575
Training Error (%)	0.99936	0.99999	1.58089	1.57427	2.99926
Test Error (%)	1.39431	1.82189	1.56212	1.59582	3.79107
Max Training Error (%)	6.25839	6.65651	6.73947	6.83416	17.4677
Max Test Error (%)	3.36469	5.39016	4.21988	3.45129	9.66778
R-Squared	0.99897	0.99524	0.99635	0.99496	0.98954
CC*	0.99948	0.99762	0.99817	0.99747	0.99476
CoE	0.99893	0.99517	0.99584	0.99400	0.98932
GoF (%)	96.7291	93.0474	93.5483	92.2513	89.6635
CoD	0.99897	0.99524	0.99635	0.99496	0.98954

*CC: Correlation Coefficient; CoE: Coefficient of Efficiency; GoF: Goodness of Fit; CoD: Coefficient of Determination (definitions are available in Supporting Information, Equations S3-S7).

3.2. A Molecular Perspective on Property-Related Features of OBCs

The use of the developed IMT enabled virtual synthesis of millions of scenarios of polymerization in a computationally cost-effective manner from the patterns it learned from the initially available 175 scenarios/polymerization experiments handled by the KMC simulator and generalized to build the ANNs for all other imaginable scenarios in the range of input factors covered. As a result, plots on property-related microstructural features can be obtained using the IMT tool.

As discussed earlier, $\Delta\overline{C8}\%$ is a key molecular criterion for predicting the mesophase separation tendency of OBCs in the molten state. Therefore, a detailed picture on variation of $\overline{C8}\%^{SOFT}$ and $\overline{C8}\%^{HARD}$ in terms of polymerization factors would be very useful in this regard. Figure 4 shows bivariate contour plots of $\overline{C8}\%^{SOFT}$ in terms of CC and log(CSA Level) for scenarios having different MR values of 0.05, 0.25, 0.50, 0.75, and 0.95, represented in Figure 4A, 4B, 4C, 4D, and 4E, respectively. The three-dimensional plots of $\overline{C8}\%^{SOFT}$

corresponding to the contour plots of Figure 4 are provided in Figure S1 in Supporting Information.

As defined earlier, the molecular parameter $\overline{C8\%}^{SOFT}$ is the average ratio of 1-octene moles incorporated into the soft blocks to the total amount of 1-octene and ethylene moles in the soft segments, while $\overline{C8\%}^{HARD}$ is the corresponding quantity for the hard segments. The comparison of plots in Figure 4 suggests that MR plays a key role in determining $\overline{C8\%}^{SOFT}$, in view of the fact that change in MR from 0.05 to 0.95 resulted in $\overline{C8\%}^{SOFT}$ being between ca. 2 and 48, i.e. the ultimate incorporation of 1-octene in the soft segments is ca. 50% of the amount in the feed, which obviously also depends on the other synthesis conditions to a minor degree. From the chain shuttling point of view, hard blocks contain almost exclusively ethylene units, as catalyst 2 (responsible for making hard blocks) harshly incorporate 1-octene into their structure, with reactivity ratio of 100 and 0.05 for ethylene and 1-octene, respectively. On the contrary, soft segments are supposed to be richer in 1-octene, as catalyst 1 incorporates 1-octene (and other bulky monomers) much easier than catalyst 2, reactivity ratio being 5 and 0.3 for ethylene and the alkene respectively. At a low MR values (Figure 4A), the concentration of 1-octene and thus the consumption rate are greater than those of ethylene. Therefore, the $\overline{C8\%}^{SOFT}$ assumes a high value due to dominance of 1-octene. By contrast, at a high MR value (Figure 4E), the soft segments accept more ethylene - what they inherently prefer to receive (in metallocene polyolefin synthesis all suitable single site catalysts prefer less bulky (e.g. ethylene) over bulkier monomers (e.g. 1-octene)). As a result, the $\overline{C8\%}^{SOFT}$ takes values between 2.3 to less than 3. At an intermediate level, however, where the MR is 0.50 (Figure 4C), OBC chains have $\overline{C8\%}^{SOFT}$ values in the range of 5 and 16.5. Interestingly enough, MR of 0.53 assigned to the Reference Batch in Table 1 has led to $\overline{C8\%}^{SOFT}$ of 11.86 at CC of 0.6 and Log(CSA Level) of zero, which closely resemble the corresponding values one may obtain at an identical polymerization recipe seen in Figure 4C. The broad range of $\overline{C8\%}^{SOFT}$ changes in Figure 4C compared to cases with ethylene- or 1-octene-rich feed compositions can be explained in that the incorporation of ethylene or 1-octene into the growing soft segments could be governed by the catalyst composition at an intermediate level of MR. As in Figure 4, especially in the case of Figure 4C and Figure 4D, the CC controls $\overline{C8\%}^{SOFT}$ independently of Log(CSA Level). Overall, it can be stated that the influence of Log(CSA)-level and CC is rather small except for MR=0.50 ($\overline{C8\%}^{SOFT}$ = 5.3-16.8,

variation by a factor of 3.2) and to a smaller extent for MR=0.75 ($\overline{C8\%}^{SOFT}$ = 2.4-7.7, variation by a factor of 2.85).
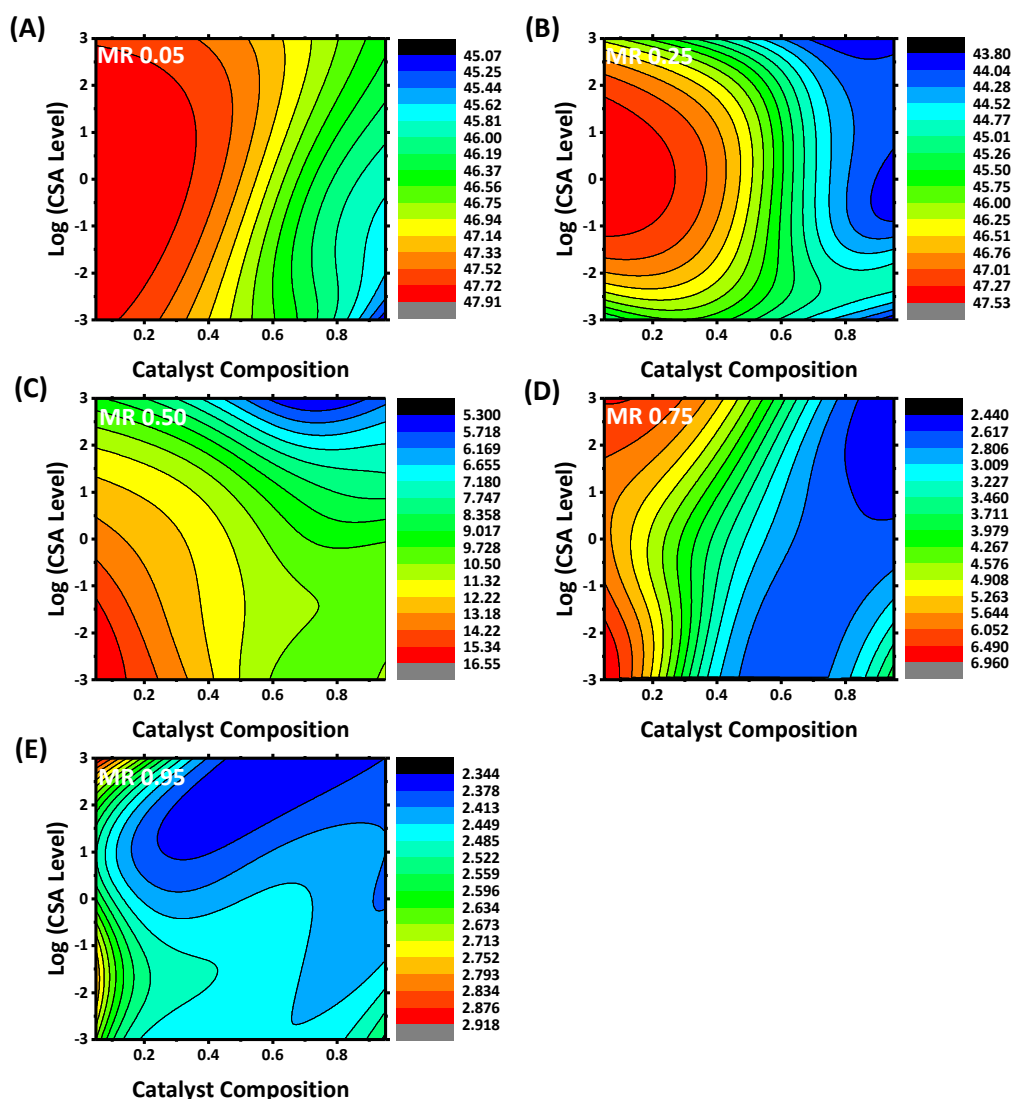

Figure 4. Bivariate contour plots of $\overline{C8\%}^{SOFT}$ in terms of CC and log(CSA level) for cases with constant MR values.

Catalyst 1 is responsible for incorporation of 1-octene into the soft blocks and, hence, assists in growing soft segments, while Catalyst 2 almost exclusively accepts ethylene, leading to the growth of hard segments. At low CC values, where Catalyst 2 is present in higher concentrations in the system relative to Catalyst 1, most of the ethylene molecules are consumed by Catalyst 2. Therefore, the soft blocks receive more 1-octene units leading to OBCs having higher values of $\overline{C8\%}^{SOFT}$. By increasing the CC value, the 1-octene units are inevitably shared between more numerous Catalyst 1 molecules;

thus, Catalyst 1 molecules producing the soft segments have less access to 1-octene, which decreases $\overline{C8\%}^{SOFT}$. However, as mentioned before, that is only a relatively minor influence for the extreme MR values, while the intermediate MR-levels (0.50 and 0.75) are strongly influenced by this effect.

It is interesting to note that the CSA Level, which is responsible for shuttling of hard and soft segments from growing species to each other, has a very limited influence on $\overline{C8\%}^{SOFT}$, except for the case shown in Figure 4E, for which the system is mostly populated with ethylene monomer units. In such a case, the determining role of CC in controlling $\overline{C8\%}^{SOFT}$ has been overshadowed by another factor, i.e. the high frequency of access to ethylene in the system. The one-shot addition of 1-octene compared to the continuous addition of ethylene into the system in the case of Figure 4E provided a much better chance of ethylene contribution to the $\overline{C8\%}^{SOFT}$ variation instead of 1-octene. As a result of this, CSA Level appeared effective to a limited extent irrespective of the CC value. In other words, the role of CC on $\overline{C8\%}^{SOFT}$ has been somehow overwhelmed by the population of ethylene in the case of Figure 4E, so that CSA Level affected $\overline{C8\%}^{SOFT}$ variation to some extent.

Figure 5 shows bivariate contour plots of $\overline{C8\%}^{HARD}$ in terms of CC and Log(CSA Level) for scenarios found by IMT at different monomer compositions. The three-dimensional plots of $\overline{C8\%}^{HARD}$ corresponding to the contour plots of Figure 5 are provided in Figure S2 of Supporting Information. The $\overline{C8\%}^{HARD}$ is calculated as the ratio of average 1-octene units incorporated into the hard blocks to the total amount of 1-octene and ethylene units in the hard blocks. Overall, in an obvious opposition to the cases of $\overline{C8\%}^{SOFT}$ in Figure 4, the MR plays a minor role in the control of $\overline{C8\%}^{HARD}$, when moving from Figure 5A to Figure 5E. It should be highlighted that the molecular variables of OBCs plotted in Figure 4 and Figure 5 are based on average values of the end-of-batch product, which are the results of two kinds of behavior being balanced over the whole time span of polymerization. For such a 'semi-batch' copolymerization, the growing chains are rich in 1-octene at an early stage of reaction, because of the fact that 1-octene was injected in an one-pot fashion into the system. Hence, both soft and hard blocks are expected to have more 1-octene units inside at the early stages of reaction. At the later stages, however, accumulation of ethylene monomer units continuously fed into the system is highly probable. Accordingly, the system would be dilute with respect to 1-octene units. In such a situation, ethylene plays the most important role in controlling 1-octene content in both blocks. Consuming relatively more 1-octene units, the

microstructural characteristics of soft blocks, especially their $\overline{C8\%}^{SOFT}$, are more sensitive to the 1-octene concentration, i.e. the MR value in the reacting system. On the other hand, as hard blocks have a lower tendency to incorporate 1-octene units, one could expect to see $\overline{C8\%}^{HARD}$ levels independent of MR.

Another key point regarding Figure 5 is that CSA Level controls the variation of $\overline{C8\%}^{HARD}$, nearly irrespective of CC. As CSA Level controls the length of both hard and soft blocks, it influences the 1-octene content in both blocks, especially in hard blocks, which stems from Catalyst 2. At high CSA Levels, the soft blocks, which have the potential to receive 1-octene, do not find enough time to propagate and quickly undergo cross-shuttling. Hence, hard blocks will have more of a chance to incorporate more 1-octene units. Furthermore, as hard blocks frequently experience cross-shuttling reactions too, they won't have enough time for elongation via incorporating more ethylene units. This means that a high $\overline{C8\%}^{HARD}$ could be expected at high CSA Levels. On the other hand, when CSA Level is low, growing chains are not amenable to chain shuttling so that soft blocks receive 1-octene at the early stages of the polymerization, when the system is full of 1-octene monomer. At the late stages of the polymerization, however, newly born chains are mainly composed of ethylene, the feedstock of such a 'semi-batch' polymerization. Due to the abundance of 1-octene units in the system and minimum possibility of shuttling, the value of $\overline{C8\%}^{HARD}$ is relatively low at lower CSA Levels. This behavior is reflected in all parts of Figure 5 irrespective of the MR levels.
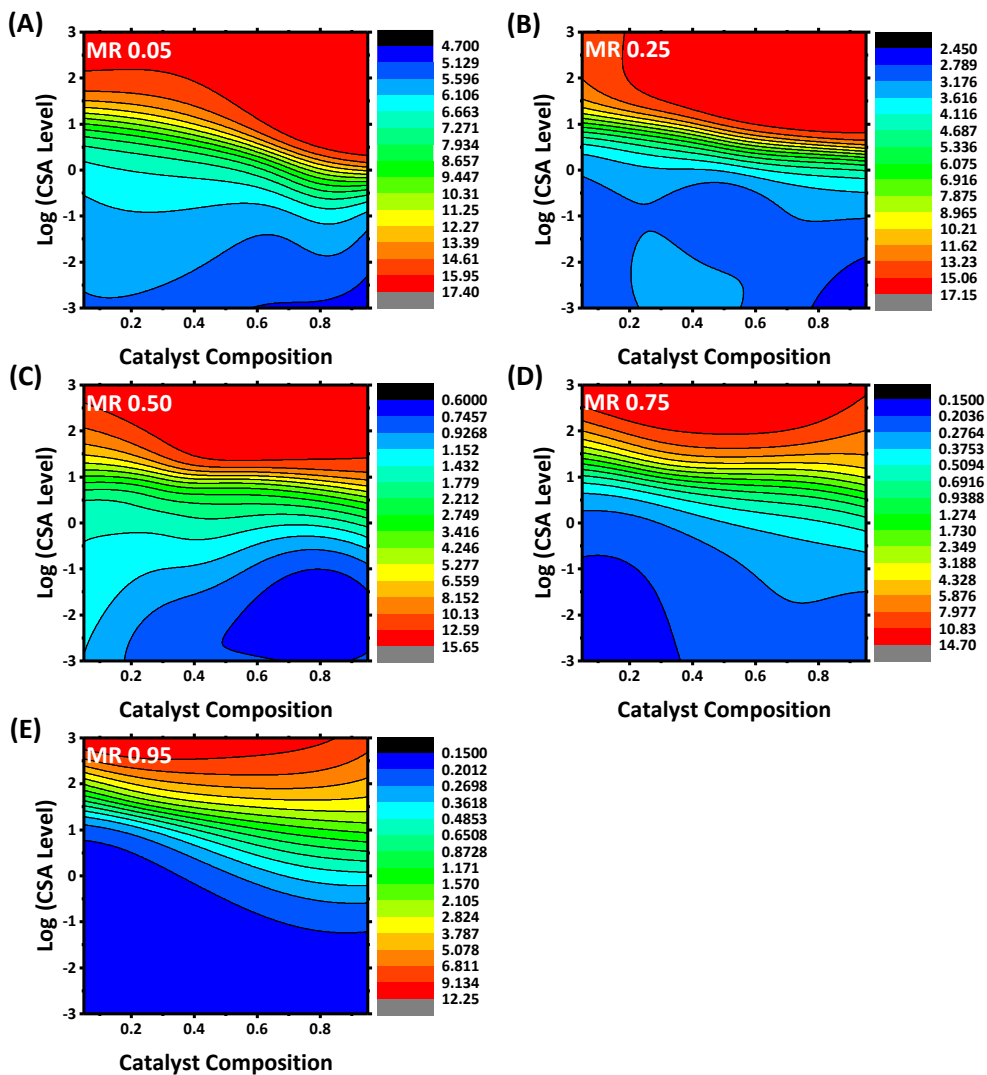
Figure 5. Bivariate contour plots of $\overline{C8\%}^{HARD}$ in terms of CC and Log(CSA Level) for cases with constant MR values.

The crystallization behavior of OBCs takes origin in the amounts of $\overline{LES}^{SOFT}$ and $\overline{LES}^{HARD}$, whose contour plots are shown in Figure 6 and Figure 7, respectively. The corresponding three-dimensional plots are provided in Figure S3 and Figure S4 of Supporting Information.
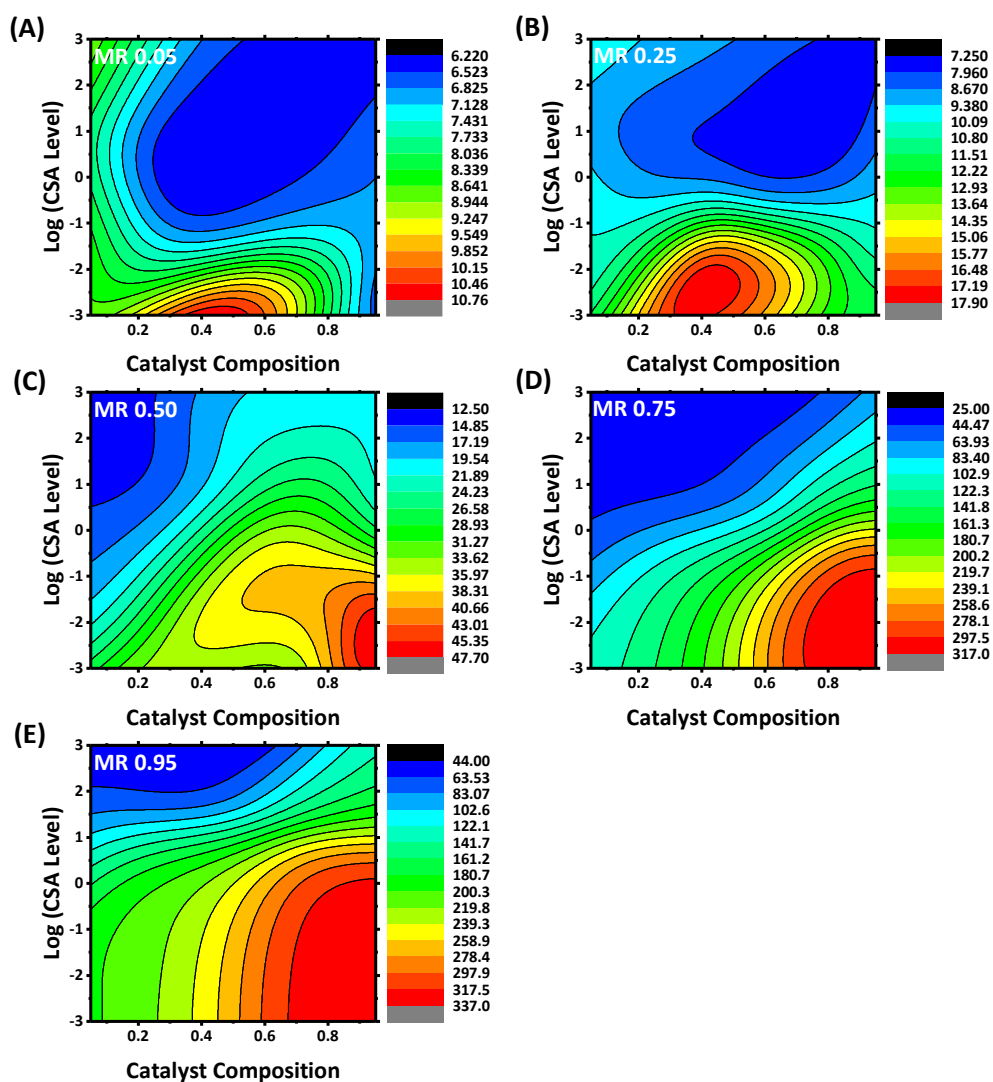
Figure 6. Bivariate contour plots of $\overline{LES}^{SOFT}$ in terms of CC and Log(CSA Level) for cases with constant MR values.

At first, one needs to understand that: (1) the LES of each block cannot be longer than the block itself, which implies a strong dependence of LES on the Log(CSA Level), and (2) the higher the relative concentration of 1-octene in the solution from which the polymers were synthesized (low MR values), the higher the likelihood that 1-octene units are incorporated. It can be understood at first glance at Figure 6 that $\overline{LES}^{SOFT}$ is very sensitive to the MR value. At low MR values, soft blocks are subjected to significant 1-octene incorporation, even though

Catalyst 1 prefers incorporating ethylene to a relatively small degree (in comparison to Catalyst 2), leading to a very low value of $\overline{LES}^{SOFT}$, as the high $\overline{C8\%}^{SOFT}$ makes long ethylene sequences in the soft segments statistically very improbable. In this case (MR=0.05, Figure 6A), the influence of the Log(CSA Level) and CC is rather small, as the variation of $\overline{LES}^{SOFT}$ is entirely governed by the MR. This in turn leaves such ethylene segments (shorter than the total block length) or the CC without a significant role. For MR=0.25 (Figure 6B), the results are similar, albeit with a slightly larger dynamic range. At high MR values, however, more ethylene monomers can be easily incorporated into the soft blocks leading to higher values of $\overline{LES}^{SOFT}$ and significantly higher larger dynamic range of 1-octene incorporation or $\overline{LES}^{SOFT}$ distribution, which is apparent in Figure 6D and Figure 6E. In such cases, the newly born chains at the later stages of the polymerization have more access to ethylene as the continuous feedstock, thanks to the higher effectiveness of Catalyst 1. Meanwhile, soft blocks of OBC chains generated in the early stages of reaction have higher 1-octene content. This contradiction results in having chains with $\overline{LES}^{SOFT}$ values ranging from about 40 to more than 340 in the case of Figure 6E with MR of 0.95. Hence, as stated earlier, the chains synthesized at high Log(CSA Level) are limited in terms of $\overline{LES}^{SOFT}$ by the block length and not by the introduction of 1-octene. Thus, it can be concluded that MR determines both the content and distribution pattern of 1-octene within the soft segments. Furthermore, it is also clear that for high Log(CSA Level), the block length is relatively short. For example, as reported previously [16] at Log(CSA Level)=3 and MR=0.95, the number average degree of polymerization $\overline{DP_n}^{SOFT}$ is between 120 and 180. Even though the blocks are not monodisperse in length, their distribution is relatively narrow, as shown in [16].

On the other hand, the CC controls the distribution profile of $\overline{LES}^{SOFT}$. At high CC values, OBCs are mostly softened, which is consistent with the tendency of Catalyst 1 for ethylene incorporation. Meanwhile, chains with soft segments formed at the early stages have more 1-octene in their structure. This irregularity causes a broad distribution observed for $\overline{LES}^{SOFT}$. Moreover, CC influences the patterns for high $\overline{LES}^{SOFT}$ (above ca. 30). A high CC means that the likelihood of self-shuttling of chains is higher and, consequently, the segments are longer, as can be seen from $\overline{DP_n}^{SOFT}$ [16]. In addition, the aforementioned argument for CSA-level

20

(limitation of $\overline{LES}^{SOFT}$ by segment length) also applies to CC, although to a smaller degree as the effect is weaker. Nevertheless, one should not ignore that at high CC, the soft segments are considerably longer than at low CC under otherwise identical conditions.

A similar but more accentuated trend can be seen for $\overline{LES}^{HARD}$ in Figure 7. For all plots, a very clear variation of $\overline{LES}^{HARD}$ with CSA-level can be observed, which has the same reasons as discussed for the soft segments. According to Figure 7, MR appears more influential at low Log(CSA)-levels; a MR of 0.95 leads to a large change in $\overline{LES}^{HARD}$ from 20 to more than 4320 (Figure 7E). Since hard segments tend to incorporate more 1-octene inside them, especially at lower CC values, at situations where the system is populated with ethylene, the possibility of 1-octene incorporation is very high; meanwhile, the difference in 1-octene content of short and long chains in the systems is high. This leads to more diversity in the case of $\overline{LES}^{HARD}$ at high MR values compared to $\overline{LES}^{SOFT}$. It should also be emphasized that the role of CSA Level on the $\overline{LES}^{HARD}$ is more significant with respect to what was seen for the case of $\overline{LES}^{SOFT}$. To some degree, such a difference between quantities of hard and soft segments was also observed for $\overline{C8\%}$ discussed earlier. This meaningful difference in the case of $\overline{LES}$ can be explained in that for C8% the quantities of hard and soft segments were solely fueled by the 1-octene content of hard or soft blocks, while for $\overline{LES}$ both the content and distribution fashion of 1-octene throughout the soft and hard segments could be of importance. Moreover, C8% is an average value determined 'intelligently' by the IMT taking into account all the $\overline{ESL}$ values of chains, while $\overline{LES}$ is a criterion that takes the highest $\overline{ESL}$ of the soft or hard segments.
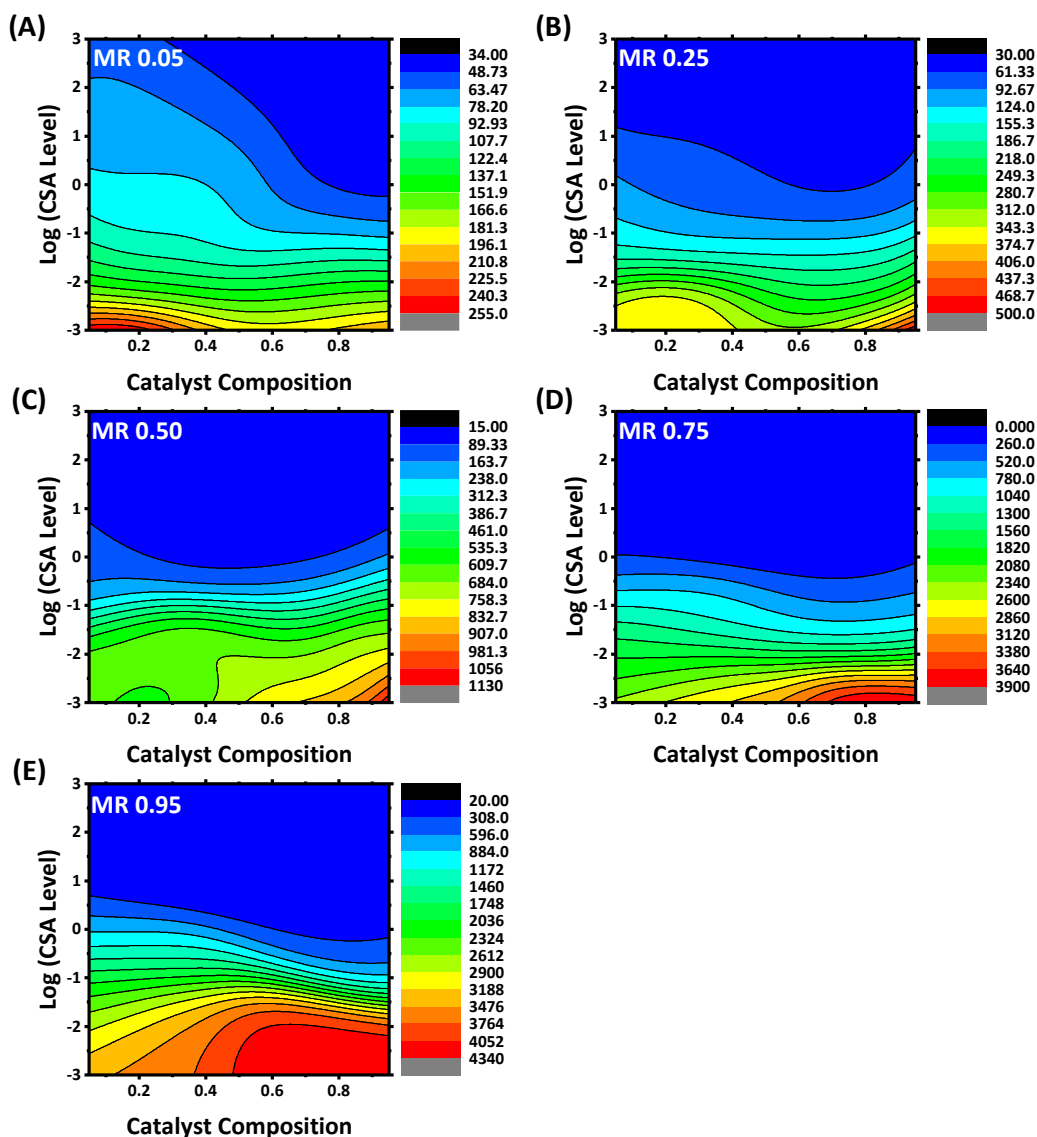
Figure 7. Bivariate contour plots of $\overline{LES}^{HARD}$ in terms of CC and Log(CSA Level) for cases with constant MR values.

Figure 8 shows variation of $HB\%$ in terms of CC and CSA Level for cases having different MR values. As expected, the amount of $HB\%$ is solely determined by the CC. The three-dimensional plot of $HB\%$ corresponding to the contour plots of Figure 8 is provided in Figure S5 of Supporting Information. At low CC values, where Catalyst 2 is predominantly introduced to the polymerization media, 1-octene could easily incorporate into the growing hard segments, leading to higher values of $HB\%$. It has been well documented that mesophase

separation of OBCs in the molten state has a rheological origin. Although the $\overline{\Delta C8\%}$ values reflect such a tendency, the quantity of $HB\%$ determines the temperature at which mesophase separation takes place.

Molecular characteristics discussed in this section, referred to as property-related characteristics of OBCs, can appropriately provide one with a deeper understanding of structure-property relationship for tailoring OBCs. The possibility of having OBCs with specified property-related characteristics has been studied and demonstrated in Figure S6 to Figure S10 of Supporting Information.
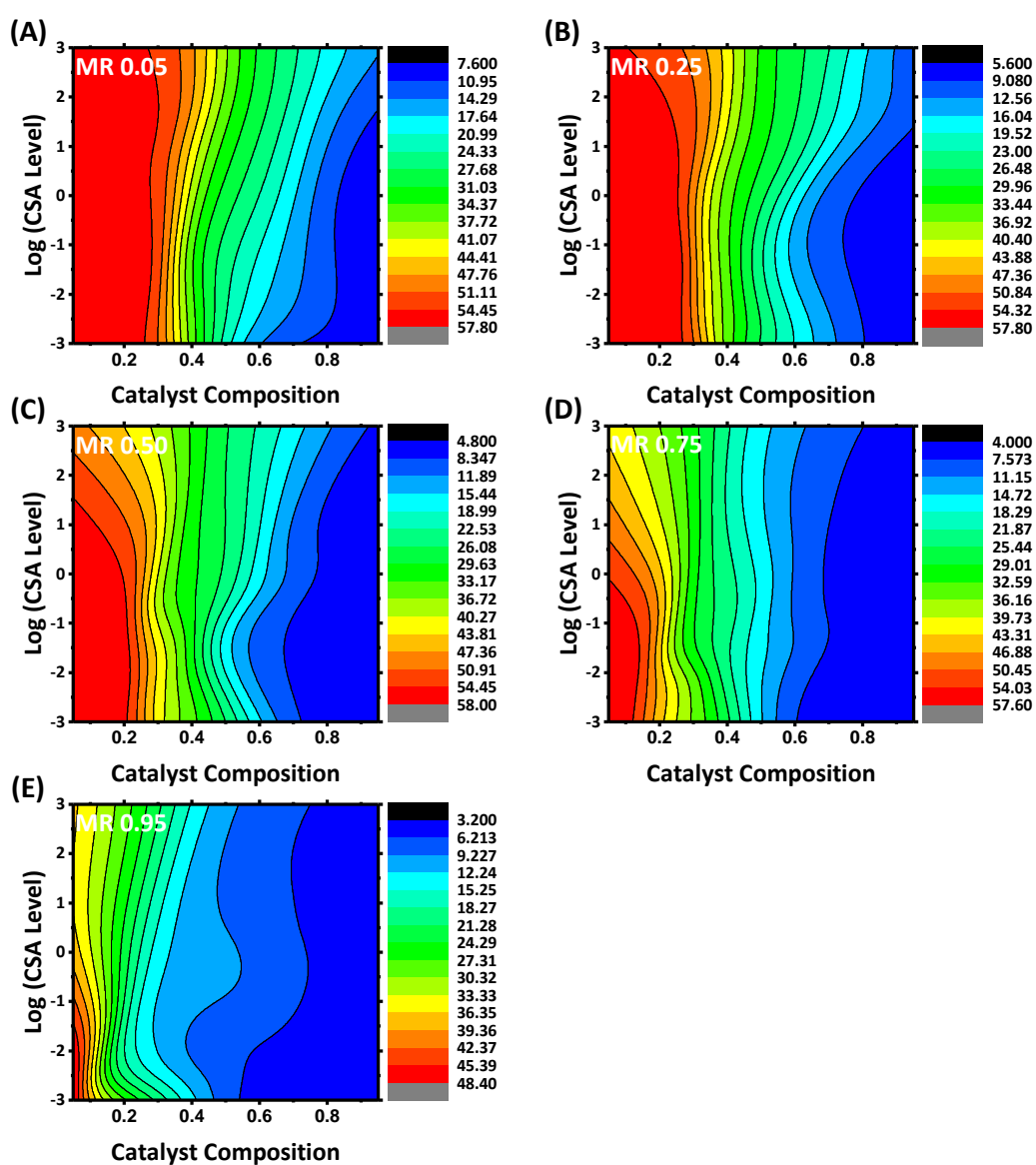
Figure 8. Bivariate contour plots of $HB\%$ in terms of CC and Log(CSA Level) for cases with constant MR values.

3.3. Tailoring the Properties of OBCs

The IMT developed in this work enabled tailoring the properties of OBCs with quite a low error in predictions. Figure 9 shows master plots representing the property-related characteristics of OBCs obtained at two different monomer ratios of 0.25 and 0.75, respectively, comprehensively discussed in previous sections. These master plots, comprising five property-related microstructural characteristics of $\overline{C8\%}^{SOFT}$, $\overline{C8\%}^{HARD}$, $\overline{LES}^{SOFT}$, $\overline{LES}^{HARD}$, and $HB\%$, are utilized to study two different grades of OBCs with specified polymerization recipes (scenarios 59 (left) and 129 (right) previously synthesized by the KMC simulator and given in Table 1), even though they can be easily employed for all other scenarios with monomer ratios of 0.25 and 0.75, respectively. For a better understanding of the predictability of the developed IMT, statistical metrics are summarized in Table 3. For each property-related feature, the difference in the lowest value (LV) and the highest value (HV) of that particular molecular characteristic was used to find the maximum deviation. The relative error in prediction of the target microstructural feature in percent was defined as the quotient of the absolute difference in outcomes of the IMT model and the KMC simulator to the absolute value of the maximum possible deviation, for that particular microstructural characteristic ($|HV - LV|$). For example, in spite of the large value range of $|HV - LV|$ for $\overline{LES}^{HARD}$, an error of less than 2% in predictions is very promising. Furthermore, and even more importantly, the master plots can be utilized in an inverse way to determine polymerization recipes needed for production of OBCs with desired mesophase separation, crystallization, or mechanical properties. To do this, at a specified MR, the amount of one of the properly-related microstructural features of the desired OBC, $HB\%$ for instance, can be fixed. Then, the corresponding master plot determines the CC and Log(CSA Level) needed for development of OBCs having the target $HB\%$. Then, other property-related variables, including $\overline{C8\%}^{SOFT}$, $\overline{C8\%}^{HARD}$, $\overline{LES}^{SOFT}$, and $\overline{LES}^{HARD}$, can be obtained at operating conditions identical to those with the preset $HB\%$. Accordingly, the final properties of OBCs can be precisely tailored using the developed IMT.
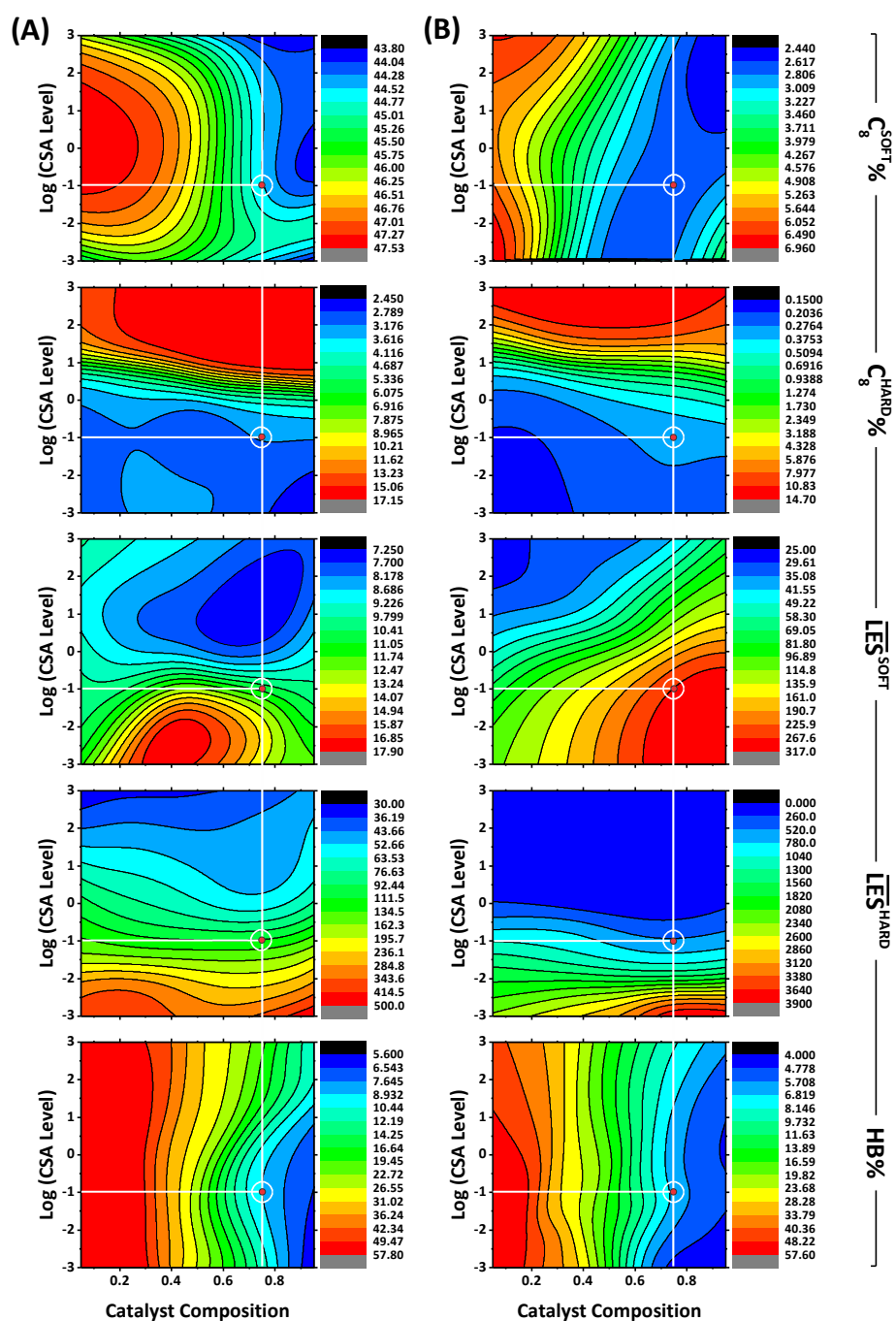
24

Figure 9. Master plots proposed and constructed by the developed IMT for manipulation of property-related microstructural characteristics of OBCs: A) the 59th scenario and (B) the 129th scenario.

Table 3. Predictability of IMT for typical scenarios, i.e. the 59th and 129th scenarios previously suggested by the KMC simulator (Table 1). Catalyst Composition: 0.75 and Log(CSA Level): -1.00.

	Scenario	MR	Y1: $\overline{C8\%}^{SOFT}$	Y2: $\overline{C8\%}^{HARD}$	Y3: $\overline{LES}^{SOFT}$	Y4: $\overline{LES}^{HARD}$	Y5: $HB\%$
ANN	59	0.25	43.18	2.89	14.75	142.27	10.63
	129	0.75	3.14	0.21	263.58	630.47	5.27
KMC	59	0.25	44.55	3.20	10.87	115.62	8.92
	129	0.75	2.68	0.31	270.58	565.71	6.50
LV		-	1.89	0.12	3.29	5.84	1.35
HV		-	50.72	17.90	347.30	4480.15	58.38
Error (%)	59	0.25	2.81	1.74	1.13	0.59	2.99
	129	0.75	0.94	0.56	2.03	1.45	2.16

3.4. Development of OBCs with Controlled Properties

Visualization of variation patterns of property-related molecular characteristics enables a deeper understanding of variations in thermal, rheological, and mechanical properties of OBCs in terms of preparation conditions. As emphasized earlier, there is a need for correlating polymerization recipe with final properties of OBCs. The use of property-related molecular features provides with some new insights into the possibility of obtaining OBCs with well-controlled properties. From the left- to right-hand side, the top row in Figure 10 illustrates 3D-views of $\overline{C8\%}^{SOFT}$ and $\overline{C8\%}^{HARD}$ as a function of Log(CSA Level) and CC for OBCs synthesized virtually at MR values of 0.50, 0.75, and 0.95, respectively. It is evident that it is possible to have OBCs for which $\overline{C8\%}^{SOFT}$ and $\overline{C8\%}^{HARD}$ are equal. In the third row, the intersection (i.e. $\overline{C8\%}^{SOFT}$ = $\overline{C8\%}^{HARD}$) is obtained and marked by a thick black line. Regardless of MR value (0.50, 075, or 0.95), the red areas in Figure 10 show OBCs with $\overline{C8\%}^{HARD}$ > $\overline{C8\%}^{SOFT}$, whereas the green areas confirm that it is possible to have OBCs for which $\overline{C8\%}^{HARD}$ < $\overline{C8\%}^{SOFT}$. The last row in Figure 10 shows the variation of $\overline{C8\%}^{SOFT}$ = $\overline{C8\%}^{HARD}$ as a function of MR. It should be noted that the CC and Log(CSA Level) variation range, which is quite broad in this work, does not allow for having OBCs with $\overline{C8\%}^{SOFT}$ = $\overline{C8\%}^{HARD}$ when MR takes on values equal or below 0.25. Figure S11 of Supporting Information may give a clearer sense of the possibility of producing OBCs having $\Delta\overline{C8\%}$ quantities very close to zero through 3D plots.

In agreement with explanations concerned with Figure 4 and Figure 5, and considering the fact that the CC and Log(CSA Level) are the main factors, respectively, responsible for controlling $\overline{C8\%}^{HARD}$ and $\overline{C8\%}^{SOFT}$, production of OBCs with equal $\overline{C8\%}^{SOFT}$ and $\overline{C8\%}^{HARD}$ would be interesting. Though no experimental report exists on studying crystallization behavior of such a specific grade of OBC for $\Delta\overline{C8\%}$ nearly zero, it can be speculated that mesophase separation would not be the lone mechanism controlling phase separation behavior of such particular grades of OBCs. As explained in the previous section, the master plots can suggest polymerization recipes required for synthesis of such specific grades of OBCs.
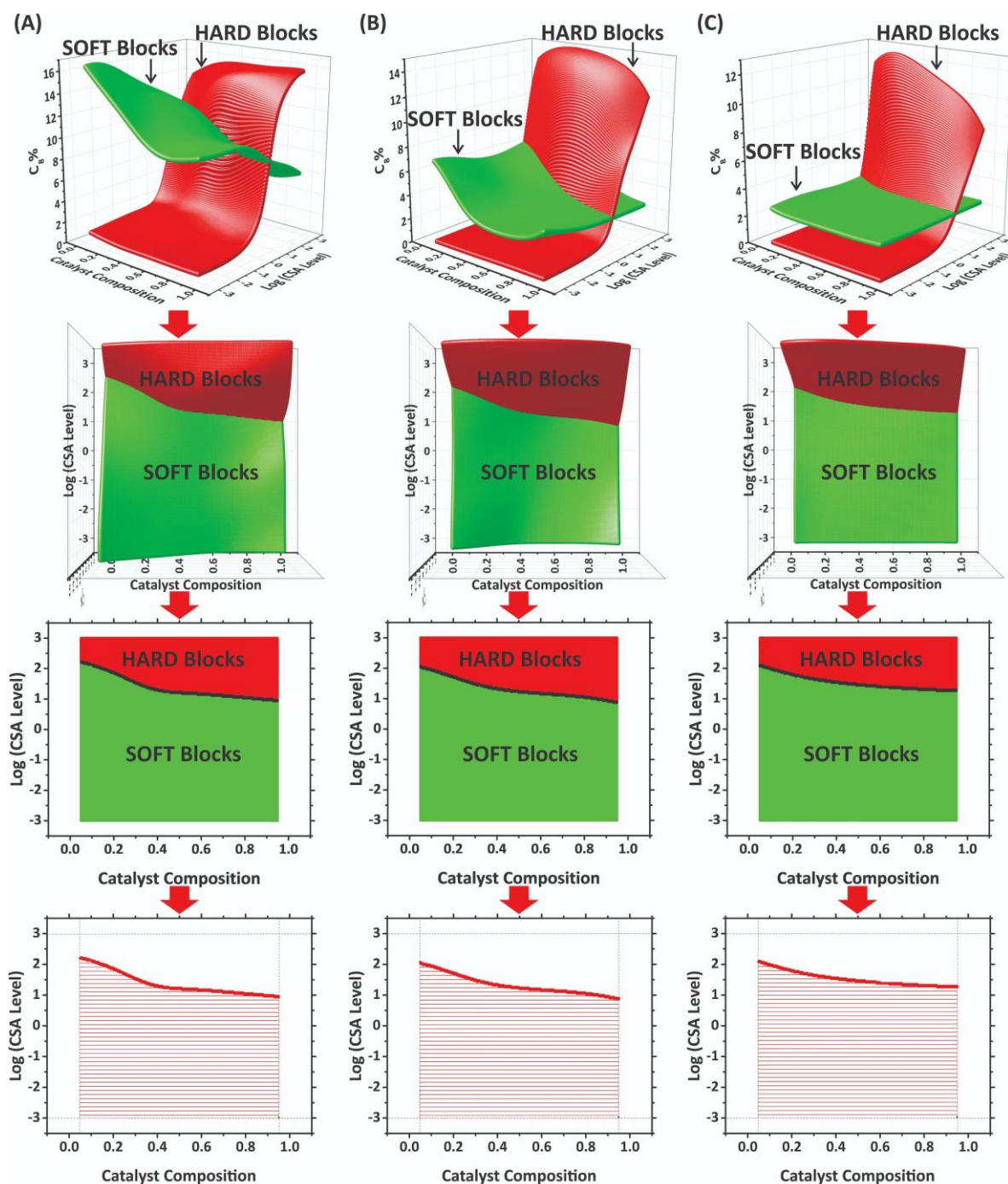
Figure 10. Analysis of possibilities of having OBCs in which $\overline{C8\%}^{SOFT}$ and $\overline{C8\%}^{HARD}$ are equal, in terms of operating conditions for cases with constant MR value of 0.50 (left column); 0.75 (middle column), and 0.95 (right column).

In a similar manner, the possibilities of having OBCs with $\overline{LES}^{SOFT}$ equal to or lower/higher than that of $\overline{LES}^{HARD}$ are evaluated with simultaneous representation (2D plots) of $\overline{LES}^{SOFT}$ and $\overline{LES}^{HARD}$ in Figure 11 and 3D illustrations in Figure S12 of Supporting Information. Again

it can be seen that MR values equal to or lower than 0.25 cannot lead to OBCs with $\overline{LES}^{SOFT}$ = $\overline{LES}^{HARD}$. This is mostly due to the fact that the lack of ethylene at low MR values keeps $\overline{LES}^{SOFT}$ low, while the low 1-octene uptake capability of catalyst 2 determines $\overline{LES}^{HARD}$ to follow an almost identical behavior over the CSA concentration. For OBCs with $\overline{LES}^{SOFT}$ and $\overline{LES}^{HARD}$ variations shown in Figure 11, the possibility of crystallization can be assessed in different zones with $\overline{LES}^{SOFT}$ equal to or lower/higher than that of $\overline{LES}^{HARD}$.
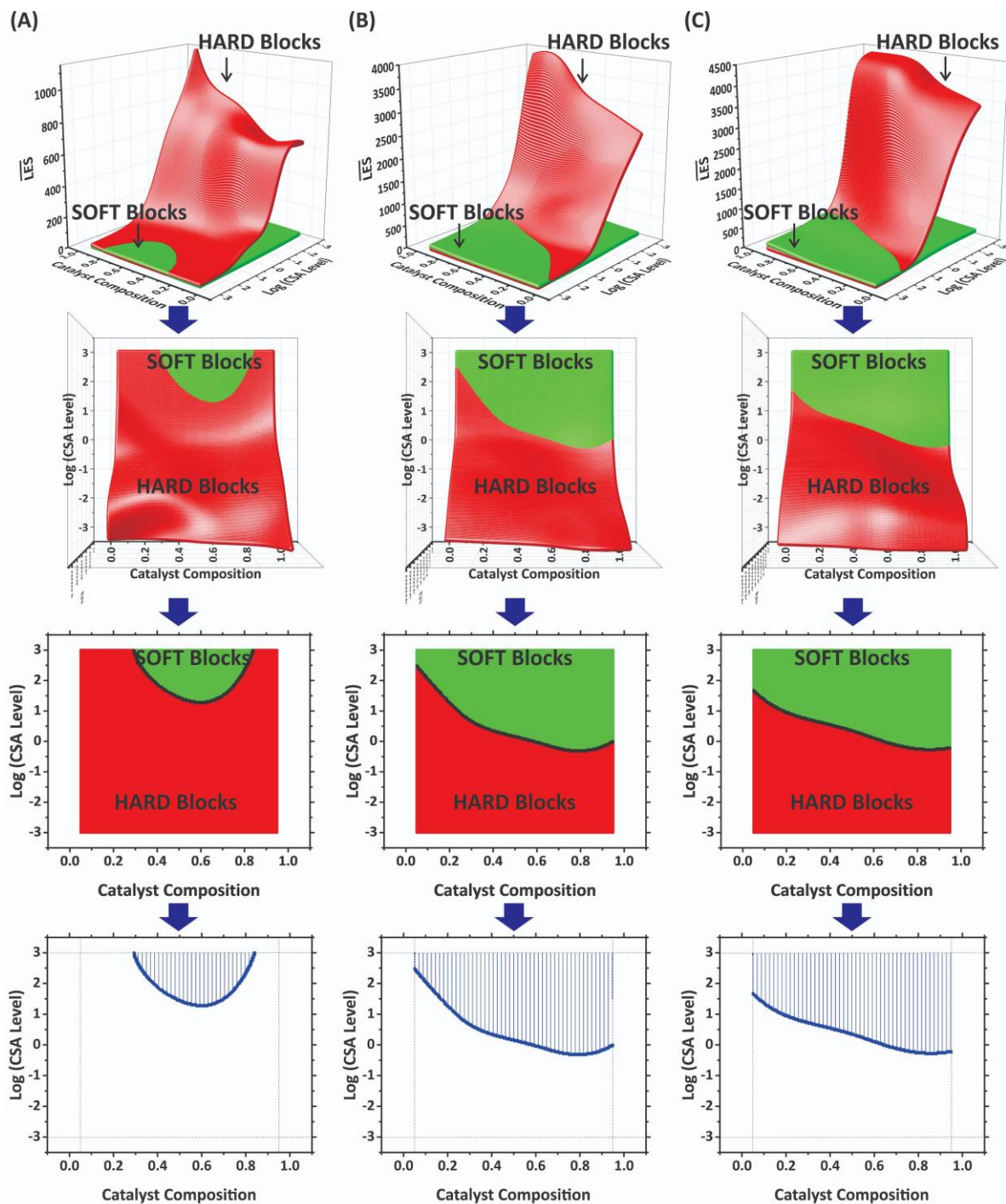
Figure 11. Analysis of possibilities of having OBCs in which $\overline{LES}^{SOFT}$ and $\overline{LES}^{HARD}$ are equal, in terms of operating conditions for cases with constant MR value of 0.50 (left column); 0.75 (middle column), and 0.95 (right column)

The next step in development of OBCs with controlled properties would be to control all the above mentioned property-related features simultaneously. The possibility of controlling $\overline{C8\%}^{HARD}$, $\overline{C8\%}^{SOFT}$, $\overline{LES}^{SOFT}$ and $\overline{LES}^{HARD}$ has been assessed as shown in Figure 12. The

figure addresses the polymerization recipe to be applied in production of OBCs with desired property-related molecular characteristics. For instance, the specific OBC coded as SOBC in Figure 12B is expected to possess a very unique crystallinity and mesophase separation behavior. The polymerization conditions needed for production of the SOBC have been proposed by the developed IMT tool. This was possible because of hybridizing the KMC and ANN approaches that intelligently synthesized plenty of scenarios to yield such useful master plots. When one property-related feature overlaps with the other, this means that it is possible, for example, to control both crystallinity and mesophase separation behavior by a single 'one-pot' copolymerization of ethylene and 1-octene at the proposed conditions. It is generally accepted that OBCs show upper critical solution temperature (UCST) type phase diagram. Thus, at low temperatures the possibility of mesophase separation is high. Possible morphologies proposed for OBCs are dot-like domains, rod-like domains and island-like texture. Such kinds of morphologies determine the crystallization rate from the molten state. Understanding the relationships between property-related molecular features of $\overline{C8\%}^{HARD}$, $\overline{C8\%}^{SOFT}$, $\overline{LES}^{SOFT}$ and $\overline{LES}^{HARD}$ uncovered in Figure 12 makes it possible to keep the properties of OBCs under good control.

Furthermore, considering that the $\overline{C8\%}^{HARD} = \overline{C8\%}^{SOFT}$ line is approximately constant, while the $\overline{LES}^{SOFT} = \overline{LES}^{HARD}$ line progresses systematically to higher log(CSA)-levels with increasing MR levels, we can suppose that for MR between ca. 0.55 and 0.9 other types of SOBC could be found at different CC values. Hence, it would be possible to produce a whole family of SOBCs with varying overall comonomer content, allowing for a detailed study of the crystallization behavior of this interesting and unprecedented class of OBCs.
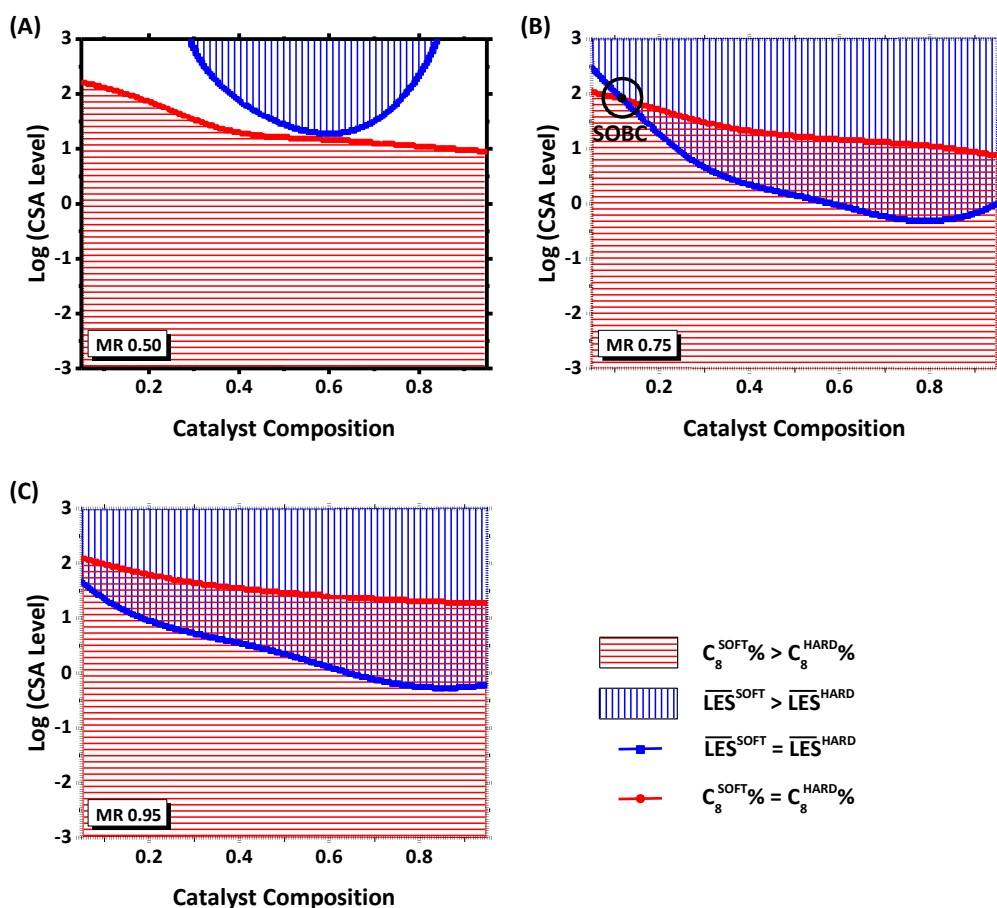
Figure 12. OBCs synthesized using IMT at constant MR values of A) 0.5, B) 0.75, and C) 0.95, with distinguished areas in which property-related characteristics take on the values cited.

There are also some cases for which the length of ethylene sequence is sufficient, but overall the content of hard blocks is low. Thus, the multitude and junctures of HB% with $\overline{C8\%}^{HARD}$, $\overline{C8\%}^{SOFT}$, $\overline{LES}^{SOFT}$ or $\overline{LES}^{HARD}$ play an important role in determining the possibility of controlling properties of OBCs (as observed in Figure 13).
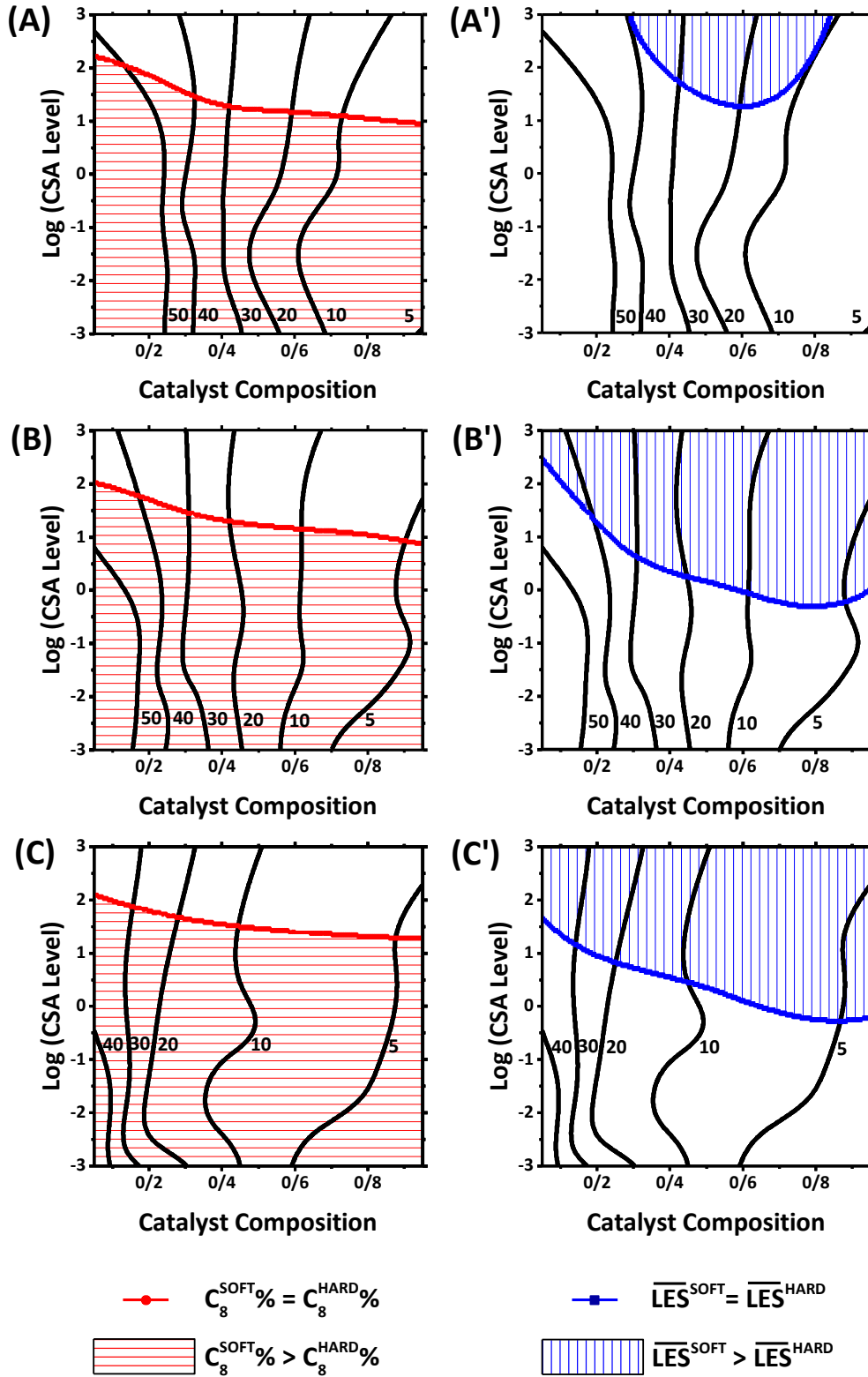
Figure 13. Junctures of property-related characteristics due to IMT: MR values of (A,A') 0.5, (B,B') 0.75, and (C,C') 0.95.

4. CONCLUSION

A machine learning-assisted KMC simulation technique is implemented and applied to 'crack' the complexity of the recipe-microstructure-property interrelationships in OBCs. To achieve this, a versatile KMC simulator capable of imitating the chain shuttling reactions and virtually synthesizing OBCs is developed, and subsequently applied to generate a large theoretical dataset on living coordination copolymerization of ethylene and 1-octene. The produced data set is employed to train several neural networks capable of precisely predicting the property-related microstructural characteristics of OBCs including the comonomer content of the soft and hard segments, the average longest ethylene sequence length of the soft and hard blocks, and hard block percentage.

The proposed intelligent model is capable of exploring the connection between polymerization recipe (catalyst composition, ethylene to 1-octene monomer ratio, and chain shuttling agent level) and property-related microstructural features. The final properties of desired OBCs are reflected in the hard block percent, the number of 1-octene units in the copolymer chains, and the longest ethylene sequence length of the hard and soft segments, which can be manipulated in a detailed fashion applying the proposed hybrid intelligent computational tool. It was shown that the developed tool can explore the predefined polymerization search space and model all potential copolymerization recipes needed for the production of master plots/'maps' representing the property-related characteristics of OBCs. Also, the master plots can be utilized in an inverse way to determine polymerization recipes needed for production of OBCs with desired mesophase separation, crystallization, or mechanical properties.

REFERENCES

[1] J.-F. Lutz, J. M. Lehn, E. W. Meijer, K. Matyjaszewski, Nat. Rev. Mater. 2016, 1, 16024.

[2] J.-F. Lutz, M. Ouchi, D. R. Liu, M. Sawamoto, Science 2013, 341, 1238149.

[3] H. Sun, C. P. Kabb, M. B. Sims, B. S. Sumerlin, Prog. Polym. Sci. 2019, 89, 61.

[4] T. R. Guimarães, M. Khan, R. P. Kuchel, I. C. Morrow, H. Minami, G. Moad, S. Perrier, P. B. Zetterlund, Macromolecules 2019, 52, 2965.

[5] Y. Zheng, C. Weng, C. Cheng, J. Zhao, R. Yang, Q. Zhang, M. Ding, H. Tan, Q. Fu, Macromolecules 2020, 53, 5992.

[6] D. J. Arriola, E. M. Carnahan, P. D. Hustad, R. L. Kuhlman, T. T. Wenzel, Science 2006, 312, 714.

[7] F. Alfano, H. W. Boone, V. Busico, R. Cipullo, J. C. Stevens, Macromolecules 2007, 40, 7736.

[8] A. Xiao, L. Wang, Q. Liu, H. Yu, J. Wang, J. Huo, Q. Tan, J. Ding, W. Ding, A. M. Amin, Macromolecules 2009, 42, 1834.

[9] R. Kuhlman, J. Klosin, Macromolecules 2010, 43, 7903.

[10] J. Wei, W. Zhang, R. Wickham, L. R. Sita, Angew. Chem. Int. Ed. 2010, 49, 9140.

[11] L. Pan, K. Zhang, M. Nishiura, Z. Hou, Angew. Chem. Int. Ed. 2011, 50, 12012.

[12] C. Descour, T. J. J. Sciarone, D. Cavallo, T. Macko, M. Kelchtermans, I. Korobkov, R. Duchateau, Polym. Chem. 2013, 4, 4718.

[13] A. Valente, G. Stoclet, F. Bonnet, A. Mortreux, M. Visseaux, P. Zinck, Angew. Chem. Int. Ed. 2014, 53, 4638.

[14] M. Zhang, T. W. Karjala, P. Jain, Ind. Eng. Chem. Res. 2010, 49, 17, 8135.

[15] Y. Mohammadi, M. R. Saeb, A. Penlidis, E. Jabbari, F. J. Stadler, P. Zinck, K. Matyjaszewski, Polymers 2019, 11, 579.

[16] M. R. Saeb, Y. Mohammadi, T. S. Kermaniyan, P. Zinck, F. J. Stadler, Polymer 2017, 116, 55.

[17] S. Li, R. A. Register, Macromolecules 2012, 45, 5773.

[18] P. He, W. Shen, W. Yu, C. Zhou, Macromolecules 2014, 47, 807.

[19] J. Fan, Q. Zhang, J. Feng, Phys. Chem. Chem. Phys. 2015, 17, 16158.

[20] G. Liu, X. Zhang, X. Li, H. Chen, K. Walton, D. Wang, J. Appl. Polym. Sci. 2012, 125, 666.

[21] J. Jin, J. Du, Q. Xia, Y. Liang, C. C. Han, Macromolecules 2010, 43, 24, 10554.

[22] Y. Zhao, Y. Zhu, G. Sui, F. Chen, Q. Zhang, Q. Fu, RSC Adv., 2015, 5, 82535.

[23] Z.-Z. Tong, B. Zhou, J. Huang, J.-T. Xu, Z.-Q. Fan, Macromolecules 2014, 47, 1, 333.

[24] J. Fan, Q. Zhang, D. Hu, J. Feng, Ind. Eng. Chem. Res. 2016, 55, 13, 3782.

[25] T. Wen, G. Liu, Y. Zhou, X. Zhang, F. Wang, H. Chen, J. Loos, D. Wang, Macromolecules 2012, 45, 15, 5979.

[26] A. Radulescu, G. Goerigk, L. Fetters, D. Richter, J. Appl. Crystallogr. 2015, 48, 1860.

[27] Q. Zhang, J. Fan, J. Feng, CrystEngComm, 2016, 18, 1532.

[28] X. Zhou, J. Feng, D. Cheng, J. Yi, L. Wang, Polymer 2013, 54, 4719.

[29] T. Wen, Y. Zhou, G. Liu, F. Wang, X. Zhang, D. Wang, H. Chen, K. Walton, G. Marchand, J. Loos, Polymer 2012, 53, 529.

[30] Y. Zhao, C. Yao, T. Chang, Y. Zhu, Polymers 2019, 11, 552.

[31] S. Anantawaraskul, P. Somnukguande, J. B. P. Soares, Macromol. Symp. 2009, 282, 205.

[32] S. Gondo, S. Osawa, H. Marubayashi, S. Nojima, Polym. J. 2015, 47, 556.

[33] Y. Mohammadi, M. Ahmadi, M. R. Saeb, M. M. Khorasani, P. Yang, F. J. Stadler, Macromolecules 2014, 47, 4778.

[34] M. R. Saeb, M. M. Khorasani, M. Ahmadi, Y. Mohammadi, F. J. Stadler, Polymer 2015, 76, 245.

[35] M. Ahmadi, M. R. Saeb, Y. Mohammadi, M. M. Khorasani, F. J. Stadler, Ind. Eng. Chem. Res. 2015, 54, 8867.

[36] M. Hosseinnezhad, M. R. Saeb, S. Garshasbi, Y. Mohammadi, Solar Energy 2017, 149, 314.

[37] B. Baghaei, M. R. Saeb, S. H. Jafari, H. A. Khonakdar, B. Rezaee, V. Goodarzi, Y. Mohammad, J. Appl. Polym. Sci. 2017, 134, 45145.

[38] Y. Mohammadi, A. Penlidis, Adv. Theory Simul. 2019, 2, 1800144.

[39] R. Azari, S. Garshasbi, P. Amini, H. Rashed-Ali, Y. Mohammadi, Energy Build. 2016, 126, 524.

[40] Y. Mohammadi, M. R. Saeb, A. Penlidis, E. Jabbari, P. Zinck, F. J. Stadler, K. Matyjaszewski, Macromol. Theory Simul. 2018, 27, 1700106.

[41] M. Ataeefard, Y. Mohammadi, M. R. Saeb, Polym. Sci. Ser. A 2019, 61, 667.